Provisional chapter

A Statistical Approach for Wave-Height Forecast Based on Spatiotemporal Variation of Surface Wind

Tsukasa Hokimoto

Additional information is available at the end of the chapter

1. Introduction

For accurate wave-height forecasts, it is necessary to take into account changes in various physical phenomena related to meteorology, because wave motion is affected by changes in ocean wind. However, it is generally difficult to carry out continuous field measurements of such physical phenomena in an area of investigation at sea, because of the lack of facilities required for such measurements. The physical processes related to meteorological or oceanographic phenomena are thought to have changeable correlations in space and time. Therefore, perhaps it is possible to forecast wave-height changes effectively by developing a method that takes spatiotemporal features into consideration. The Japan Meteorological Agency has set up regional stations for ground-based meteorological monitoring of coastal areas using ultrasonic wave-height meters. The systems is referred to as the Automated Meteorological Data Acquisition System (AMeDAS). An approach for wave-height forecast, based on spatiotemporal wind motions monitored at multiple ground-based AMeDAS stations, provides an alternative method for solving the above measurement problem.

One of traditional approaches for analyzing wave-height changes is to regard sea surface oscillations to be a probabilistic phenomenon and then to consider statistical approaches for expressing the dynamics of wave heights from this standpoint. Statistical models for dealing with measurements of long-term variations in wave height have been considered mainly from two perspectives: nonstationarity (e.g., Scheffner and Borgman (1992), Athanassoulis and Stefanakos (1995), Guedes Soares and Ferreira (1996)) and nonlinearity (e.g., Scotto and Guedes Soares (2000)). On the other hand, statistical methods for modeling wave height that take into account changes in wind speed and wind direction have also been considered (e.g., Hokimoto and Shimizu (2008), Hokimoto (2012)). However, adequate statistical considerations of whether or not the use of spatiotemporal wind motion is an effective method for expressing and forecasting changes in wave height have not yet been undertaken.

Also, it is not clear that statistical spatiotemporal models can improve forecasting accuracy when traditional statistical models are used.

In this chapter, we consider the points above through the development of a statistical spatiotemporal model. We first consider a time series model for expressing the relationship between wave-height changes measured in a coastal area and wind motion (i.e., wind direction and wind speed) measured at a single meteorological AMeDAS station, by extending the model considered in Hokimoto and Shimizu (2008). Then we propose a method to take spatiotemporally measured wind motion data into account, by extending the model structure developed above. Also, the applicability of the method for the analysis of actual phenomena is evaluated by a case study of wave-height forecast from a coastal area of Hokkaido, Japan.

This chapter is organized as follows. In Section 2, we describe field measurements of wave height and wind motion, including a preliminary statistical analysis of the measured data. In Section 3, we develop a statistical spatiotemporal model for forecasting wave height. The effectiveness of the method is examined by forecasting experiments in Section 4. Then in Section 5, we show the applicability of the method in the analysis of actual phenomena through a case study. Conclusions are given in Section 6.

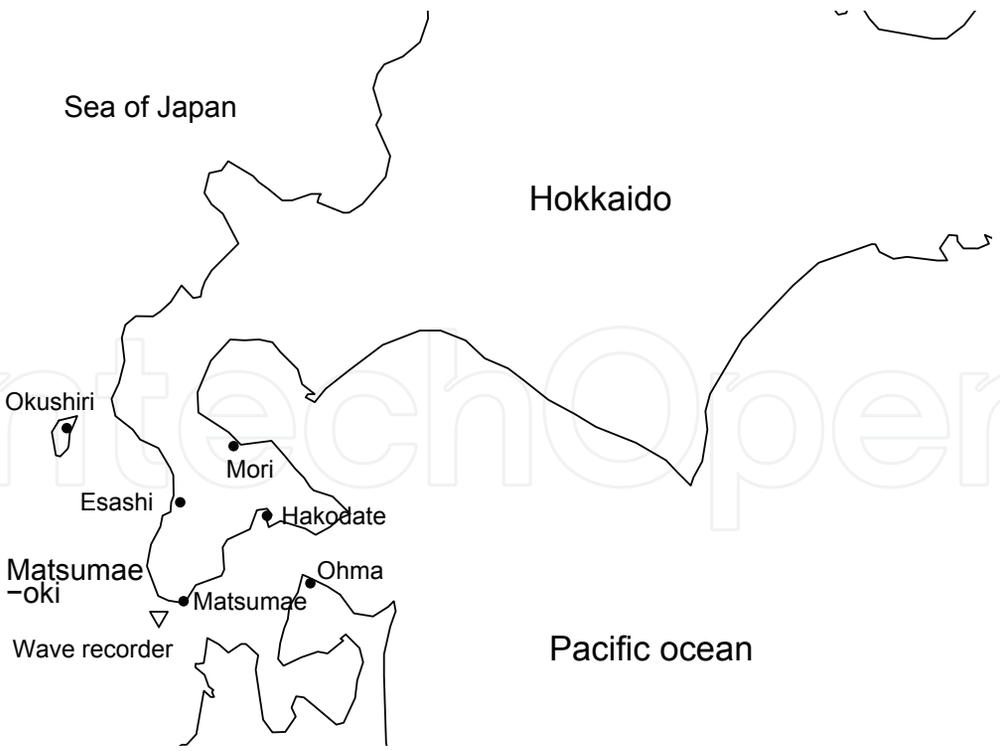

Figure 1. Locations of wave recorder and meteorological stations

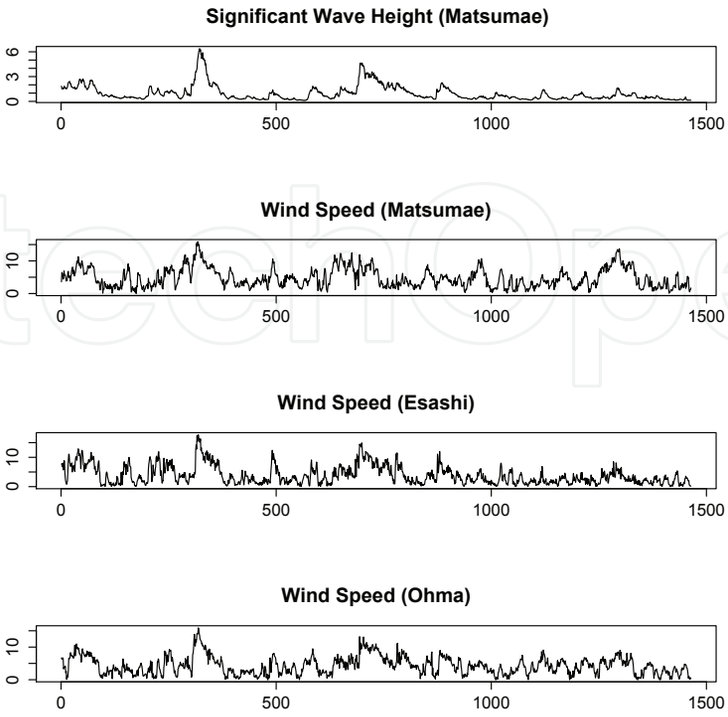

Figure 2. Wave height at Matsumae-oki and wind speeds over Matsumae, Esashi and Ohma

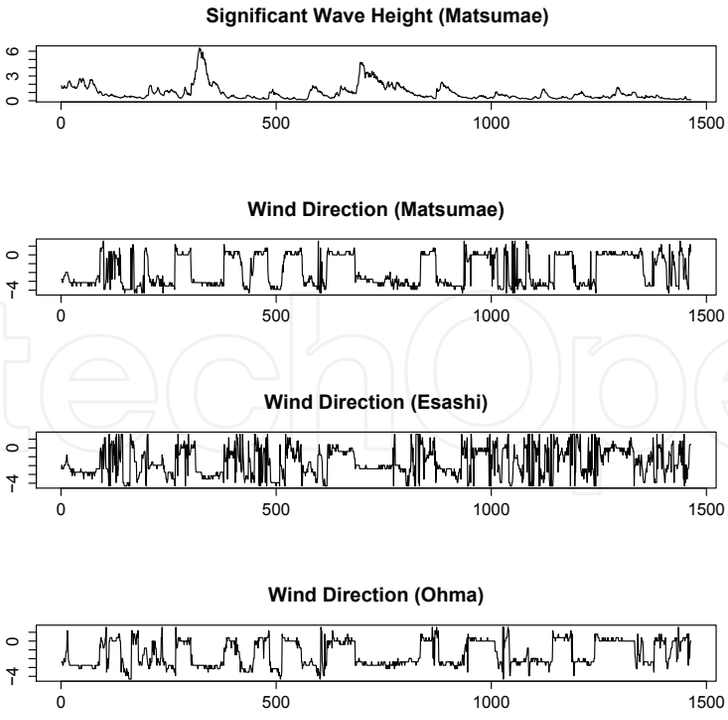

Figure 3. Wave height at Matsumae-oki and wind directions over Matsumae, Esashi and Ohma

2. Monitoring wave-height and spatiotemporal changes of wind motion

In this chapter, we consider a case study of wave-height forecast as monitored at Matsumae-oki, Hokkaido, Japan. Matsumae is a famous fisheries town where many of the local people are involved with various activities related to the sea as part of their daily lives. The neighboring area of Matsumae-oki, directly on the coast, is known for its dangerous seas. Sea conditions here quickly tend to become rough after the onset of ocean winds. In this region, wave observations using an ultrasonic wave-height metering system have been undertaken by the Japan Meteorological Agency since 1979. The sensor of the wave-height meter is located on the seabed at a depth of approximately 50 m at $42^{\circ}24'38''$N, $140^{\circ}05'50''$E. The meter measures the movement of the sea surface above using ultrasonic waves, then transmits a stream of data, including significant wave heights and wave period, to a main recording center. At the AMeDAS stations located in the neighboring area of Matsumae-oki, atmospheric properties such as temperature, precipitation, wind speed, wind direction and hours of sunlight are also measured and sent to the main center.

Figure 1 displays the location of the wave recorder and six towns in the neighboring area where AMeDAS stations are located. Also Figures 2 and 3 show an example of the measured data on 1/3 significant wave height (m), wind speed (m/s) and wind direction (rad.), for the period from April to May of 2010, where the sampling time interval is 1 hour. As noted in Figure 3, the origin of the wind direction is to the east and a positive increase corresponds to a clockwise change in direction. Since the AMeDAS station at Matsumae is closest to the wave recorder, it may be possible to use the wind motion monitored at Matsumae only, to develop a wave-height forecasting method. However, it is unclear whether this method is reasonable for expressing the dynamic structure of wave-height changes. In Figure 2, for example, it appears that the characteristics of wave-height change at Matsumae-oki are less synchronous with the wind speed changes at Matsumae, which is closest to the wave recorder, than that at Esashi, which is farther away than Matsumae. From a physical standpoint, this phenomenon can be explained by the interruption of wind flow by geographical features such as mountains.

We are interested in whether or not taking into account the spatiotemporal structure of the measured data on surface wind, monitored from the multiple AMeDAS stations, affects the forecast of wave heights. To investigate the effectiveness of introducing the class of spatiotemporal models, we have undertaken a preliminary analysis of the spatial and temporal correlation structure. Let $\{WH_t\}$, $\{WS_t\}$ and $\{WD_t\}$ be time series on 1/3 significant wave height, wind speed and wind direction, respectively. Figure 4 displays the cross correlation between the differenced time series $\{\nabla(WS_t \cos(WD_t))\}$ and $\{\nabla WH_t\}$ based on the measured data at Matsumae, Esashi and Ohma, for the three periods [150-250] (top), [300-400] (middle) and [450-550] (bottom). Here, the two dotted lines correspond to Bartlett's bounds to test the significance of the correlation between the two time series. Matsumae, Esashi and Ohma are located to the northeast, north and east of the measuring point, respectively. In [150-250], the wave-height change is most closely correlated with the wind motion over Matsumae, but the correlation gradually reduces over time. In fact, the town that gives the maximum cross-correlation value changes from Matsumae to Esashi, then to Ohma. This suggests the possibility of taking the contribution of spatiotemporal structure into account to improve the accuracy of wave-height forecasts.

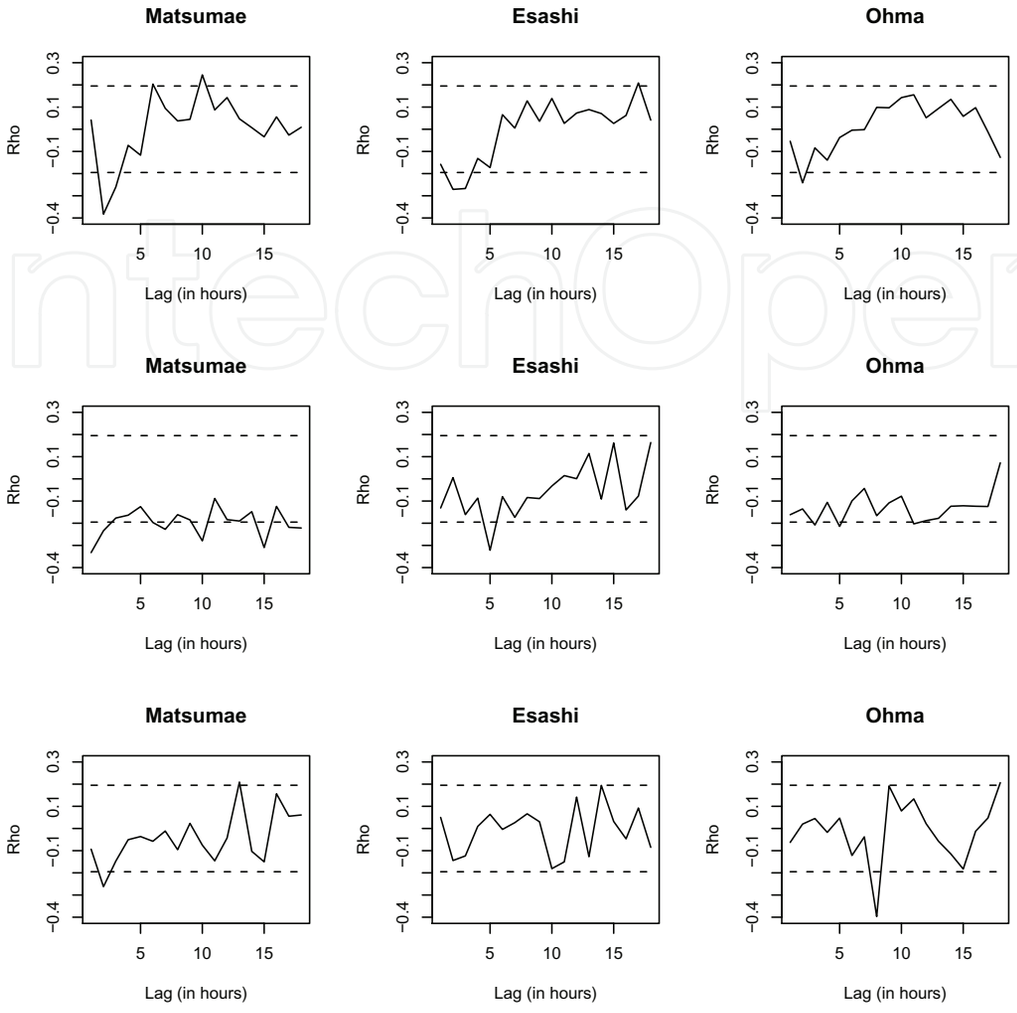

Figure 4. Change in cross correlation coefficients between $\{\nabla(WS_t \cos(WD_t))\}$ and $\{\nabla WH_t\}$ (from the top, estimated results for the periods [150-250], [300-400] and [450-500])

3. A statistical method for forecasting wave-height changes from spatiotemporal wind motion

In this section, we follow on from the result of the preliminary analysis presented in the previous section by considering the statistical spatiotemporal modeling of wave weight. As shown in Figures 2 and 3, the characteristics of the wind speed and wind direction time series are different. For this reason, different classes of time series models have been considered to express changes in wind speed and wind direction. For wind speed, linear models such as ARMA (e.g., Philippopoulos and Deligiorgi (2009)) and GARCH (e.g., Tol (1997) and Liu et al. (2011)) have been applied for analysis. In contrast, wind direction time series frequently tend to show rapid changes, which have different characteristics than those of wind speed. Johnson and Wehrly (1978) considered a linear regression model to deal with directional data and Hokimoto and Shimizu (2008) considered a time series model for the situation above. We extend the model structure of Hokimoto and Shimizu (2008) to consider the spatiotemporal relationship between wind motion and wave height. We first consider a time series model to forecast wave height based on the wind motion monitored at a single meteorological station.

Then, we extend the model so that it is applicable to the spatiotemporal wind speed and wind direction data. Our goal is to develop a predictor of wave height, WH_{T+l} ($l = 1, \ldots, L$), based on the measured data $\{WH_t\}$, $\{WS_t\}$ and $\{WD_t\}$ ($t = 1, \ldots, T$).

3.1. Forecasting wave height from surface wind over a single meteorological station

A good place to start a consideration of wave-height modeling is from forecasts of wave height from a single meteorological station. We assume that $\{WD_t\}$ ($-\pi \leq WD_t \leq \pi$) follows a von Mises process of the first order, as considered by Breckling (1989). Under this assumption, the conditional distribution under $\{WD_{t-1}\}$ is observed to follow a von Mises distribution with a mean $\mu_{(WD),t}$ and concentration $\rho_{(WD),t}$, which satisfy

$$\rho_{(WD),t} \begin{pmatrix} \cos(\mu_{(WD),t}) \\ \sin(\mu_{(WD),t}) \end{pmatrix} = k_1 \begin{pmatrix} \cos(WD_{t-1}) \\ \sin(WD_{t-1}) \end{pmatrix} + k_0 \begin{pmatrix} 1 \\ 0 \end{pmatrix}$$
$$k_0 > 0,\ k_1 > 0,\ -\pi \leq \mu_{(WD),t} \leq \pi,\ \rho_{(WD),t} > 0$$

where k_0 and k_1 are unknown parameters which take positive values. The conditional probability density function of WD_t, under WD_{t-1} is observed, can be written by

$$f(WD_t|WD_{t-1}) = \frac{1}{2\pi I_0(\rho_{(WD),t})} \exp\{k_1 \cos(WD_t - WD_{t-1}) + k_0 \cos WD_t\} \tag{1}$$

where $I_0(\cdot)$ is a modified zero-order Bessel function. (1) can be rewritten by the probability density function of the von Mises distribution

$$f(WD_t|WD_{t-1}) = \frac{1}{2\pi I_0(\rho_{(WD),t})} \exp(\rho_{(WD),t} \cos(WD_t - \mu_{(WD),t}))$$

where

$$\mu_{(WD),t} = \tan^{-1}\left(\frac{k_1 \sin(WD_{t-1})}{k_1 \cos(WD_{t-1}) + k_0}\right) \tag{2}$$

and

$$\rho_{(WD),t} = \sqrt{(k_1 \cos(WD_{t-1}) + k_0)^2 + (k_1 \sin(WD_{t-1}))^2} \tag{3}$$

which means that the parameters ($\mu_{(WD),t}$, $\rho_{(WD),t}$) change depending on (k_0, k_1) and WD_{t-1}. When both k_0 and k_1 are sufficiently small, the concentration parameter $\rho_{(WD),t}$ also becomes small and therefore (1) can be approximated by a uniform distribution. Conversely, when k_0 or k_1 becomes larger, $\rho_{(WD),t}$ also gets larger and changes to a distribution which is concentrated around $\mu_{(WD),t}$.

Next, consider a method for the estimation of the above process. To guarantee the positivity of $\rho_{(WD),t}$, we write $k_i = \exp(c_i)$ $(i = 0, 1)$ and then estimate values of the parameter (c_0, c_1). Suppose that the conditional density function of WD_t can be written by

$$f(WD_t|WD_{t-1}, \ldots, WD_1) = f(WD_t|WD_{t-1}).$$

Then the likelihood function $f(WD_1, \ldots, WD_T)$ can be written as

$$\prod_{j=2}^{T} \frac{1}{2\pi I_0(\rho_{(WD),j})} \exp\{\exp(c_1)\cos(WD_j - WD_{j-1}) + \exp(c_0)\cos(WD_j)\} \cdot f(WD_1). \quad (4)$$

(4) is a function of the parameters (c_0, c_1) only, and their values can be estimated by maximization of (4). Let $(\hat{c}_0, \hat{c}_1)$ be the maximum likelihood estimates obtained above. Then $\hat{\mu}_{(WD),t}$ and $\hat{\rho}_{(WD),t}$ can be estimated respectively by

$$\hat{\mu}_{(WD),t} = \tan^{-1}\left(\frac{\exp(\hat{c}_1)\sin(WD_{t-1})}{\exp(\hat{c}_1)\cos(WD_{t-1}) + \exp(\hat{c}_0)}\right) \quad (5)$$

and

$$\hat{\rho}_{(WD),t} = \sqrt{(\exp(\hat{c}_1)\cos(WD_{t-1}) + \exp(\hat{c}_0))^2 + (\exp(\hat{c}_1)\sin(WD_{t-1}))^2}. \quad (6)$$

Figure 5 shows a time series of the estimated value of $\{\cos(\hat{\mu}_{(WD),t})\}$, its autocorrelation and the time series $\{\hat{\rho}_{(WD),t}\}$. Note that $\{\cos(\hat{\mu}_{(WD),t})\}$ has a tendency to change in a certain range with a significant autocorrelation, and $\{\hat{\rho}_{(WD),t}\}$ exhibits nonstationarity in the sense that the mean and variance change clearly over time. Therefore, $\{\cos(\hat{\mu}_{(WD),t})\}$ and $\{\hat{\rho}_{(WD),t}\}$ can be regarded as stationary and nonstationary time series, respectively.

The modeling strategy applied here is to extend the nonstationary model structure considered by Hokimoto and Shimizu (2008) so that the new model can take into account the synchronous relationship between the von Mises process assumed for the change in wind direction. The extended model is written by

$$\begin{aligned}\nabla WH_t = &\sum_{i=1}^{p} \alpha_i^{(1)} \nabla WH_{t-i} + \sum_{i=1}^{p}\sum_{k=1}^{K} \beta_{i,k}^{(1)} \nabla(\rho_{(WD),t-i} WS_{t-i}\cos(kWD_{t-i})) \\ &+ \sum_{i=1}^{p}\sum_{k=1}^{K} \gamma_{i,k}^{(1)} \nabla(\rho_{(WD),t-i} WS_{t-i}\sin(kWD_{t-i})) + \sum_{i=1}^{p} \delta_i^{(1)}\cos(\mu_{(WD),t-i}) \\ &+ \sum_{i=1}^{p} \omega_i^{(1)}\sin(\mu_{(WD),t-i}) + \varepsilon_t^{(1)}, \quad \varepsilon_t^{(1)} \sim WN(0, \sigma_{1,h}^2)\end{aligned}$$

where p and K are orders, $(\alpha^{(1)}, \beta^{(1)}, \gamma^{(1)}, \delta^{(1)}, \omega^{(1)})$ are unknown constants and $\varepsilon_t^{(1)}$ is a random variable that follows a zero-mean white noise process.

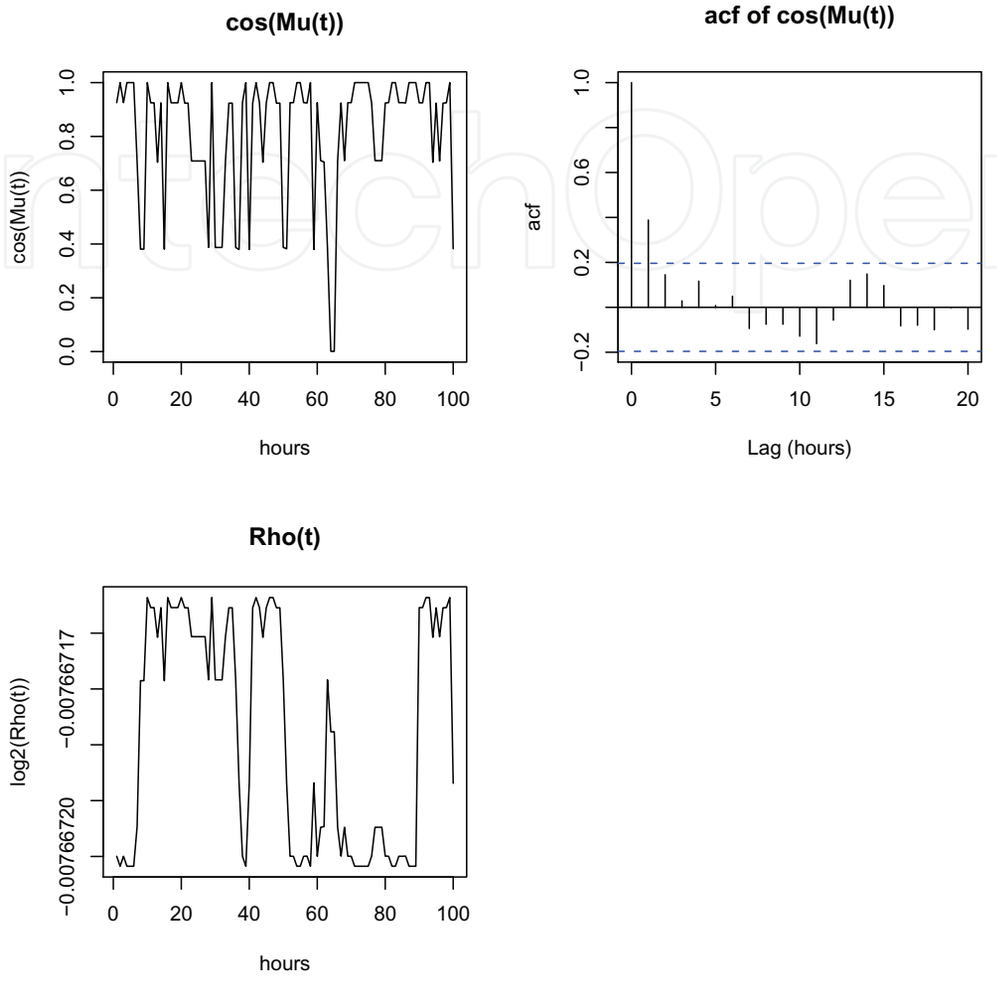

Figure 5. Time series $\{\cos(\hat{\mu}_{(WD),t})\}$ and its autocorrelation (top) and time series $\{\hat{\rho}_{(WD),t}\}$ (bottom)

Similarly, we write $\nabla(\rho_{(WD),t} WS_t \cos(hWD_t))$ and $\nabla(\rho_{(WD),t} WS_t \sin(hWD_t))$ $(h = 1, \ldots, K)$ in the form

$$\begin{aligned}\nabla(\rho_{(WD),t} WS_t \cos(hWD_t)) = &\sum_{i=1}^{p} \alpha_i^{(2)} \nabla WH_{t-i} + \sum_{i=1}^{p}\sum_{k=1}^{K} \beta_{i,k}^{(2)} \nabla(\rho_{(WD),t-i} WS_{t-i} \cos(kWD_{t-i})) \\ &+ \sum_{i=1}^{p}\sum_{k=1}^{K} \gamma_{i,k}^{(2)} \nabla(\rho_{(WD),t-i} WS_{t-i} \sin(kWD_{t-i})) + \sum_{i=1}^{p} \delta_i^{(2)} \cos(\mu_{(WD),t-i}) \\ &+ \sum_{i=1}^{p} \omega_i^{(2)} \sin(\mu_{(WD),t-i}) + \varepsilon_t^{(2)}, \quad \varepsilon_t^{(2)} \sim WN(0, \sigma_{2,h}^2)\end{aligned}$$

and $\cos(\mu_{(WD),t})$ and $\sin(\mu_{(WD),t})$ as

$$\begin{aligned}\cos(\mu_{(WD),t}) = &\sum_{i=1}^{p} \alpha_i^{(3)} \nabla WH_{t-i} + \sum_{i=1}^{p}\sum_{k=1}^{K} \beta_{i,k}^{(3)} \nabla(\rho_{(WD),t-i} WS_{t-i} \cos(kWD_{t-i})) \\ &+ \sum_{i=1}^{p}\sum_{k=1}^{K} \gamma_{i,k}^{(3)} \nabla(\rho_{(WD),t} WS_{t-i} \sin(kWD_{t-i})) + \sum_{i=1}^{p} \delta_i^{(3)} \cos(\mu_{(WD),t-i}) \\ &+ \sum_{i=1}^{p} \omega_i^{(3)} \sin(\mu_{(WD),t-i}) + \varepsilon_{t-i}^{(3)}, \ \ \varepsilon_t^{(3)} \sim WN(0, \sigma_{3,h}^2).\end{aligned}$$

A state vector at time t is defined by

$$\begin{aligned}\boldsymbol{y}_t^{(K)} \equiv &(\nabla WH_t, \ \nabla(\rho_{(WD),t} WS_t \cos(WD_t)), \ \nabla(\rho_{(WD),t} WS_t \sin(WD_t)), \ \ldots, \\ &\nabla(\rho_{(WD),t} WS_t \cos(K \cdot WD_t)), \ \nabla(\rho_{(WD),t} WS_t \sin(K \cdot WD_t)), \ \cos(\mu_{(WD),t}), \ \sin(\mu_{(WD),t}))' \quad (7)\end{aligned}$$

Then, the models given above can be unified as a multivariate AR model

$$\boldsymbol{y}_t^{(K)} = A_1^{(K)} \boldsymbol{y}_{t-1}^{(K)} + \cdots + A_p^{(K)} \boldsymbol{y}_{t-p}^{(K)} + \boldsymbol{\delta}_t^{(K)} \qquad \boldsymbol{\delta}_t^{(K)} \sim WN(\mathbf{0}, \Sigma^{(K)}) \tag{8}$$

where $A_i^{(K)}$ $(i = 1, \ldots, p)$ is an unknown coefficients matrix.

The predictor of (8) can be constructed in the following way. We first estimate (c_0, c_1) by maximizing the likelihood of (4) and then obtain the values of $\{\hat{\mu}_{(WD),t}\}$ and $\{\hat{\rho}_{(WD),t}\}$ by (5) and (6), respectively. Next, we construct the sequence of $\boldsymbol{y}_t^{(K)}$ by

$$\begin{aligned}\boldsymbol{y}_t^{(K)} \equiv &(\nabla WH_t, \ \nabla(\hat{\rho}_{(WD),t} WS_t \cos(WD_t)), \ \nabla(\hat{\rho}_{(WD),t} WS_t \sin(WD_t)), \ \ldots, \\ &\nabla(\hat{\rho}_{(WD),t} WS_t \cos(K \cdot WD_t)), \ \nabla(\hat{\rho}_{(WD),t} WS_t \sin(K \cdot WD_t)), \ \cos(\hat{\mu}_{(WD),t}), \ \sin(\hat{\mu}_{(WD),t}))'\end{aligned}$$

and then fit (8) to $\{\boldsymbol{y}_t^{(K)}\}$ $(t = 1, \ldots, T)$. A linear predictor based on (8) can be constructed by

$$\begin{aligned}\hat{\boldsymbol{y}}_{T+l}^{(K)} &= \hat{A}_1^{(K)} \boldsymbol{z}_{T+l-1}^{(K)} + \hat{A}_2^{(K)} \boldsymbol{z}_{T+l-2}^{(K)} + \cdots + \hat{A}_p^{(K)} \boldsymbol{z}_{T+l-p}^{(K)}, \\ \boldsymbol{z}_{T+l-m}^{(K)} &= \boldsymbol{y}_{T+l-p}^{(K)} (l \le p), \qquad \boldsymbol{z}_{T+l-m}^{(K)} = \hat{\boldsymbol{y}}_{T+l-p}^{(K)} (l > p)\end{aligned} \tag{9}$$

where $\hat{A}_i^{(K)}$ $(i = 1, \ldots, p)$ are the least squares estimator (e.g., Brockwell and Davis (1996)).

3.2. Forecasting wave height from spatiotemporal surface wind over multiple meteorological stations

In this subsection, we extend the method presented in 3.1 so that it is applicable to the spatiotemporal data measured at multiple meteorological stations. We continue our consideration by setting $K = 1$. Here we consider a spatiotemporal model by expressing the situation that the wind flow, which has the largest impact on wave height, changes over time. First, rather than (7), the state vector for fitting the multivariate AR model (8) is defined by

$$\boldsymbol{y}_{t|s^*} \equiv (\nabla WH_t,\ \nabla(\rho_t^{(s^*)} WS_t^{(s^*)} \cos(WD_t^{(s^*)})),\ \nabla(\rho_t^{(s^*)} WS_t^{(s^*)} \sin(WD_t^{(s^*)})),\ \cos(\mu_{(WD),t}^{(s^*)}),\ \sin(\mu_{(WD),t}^{(s^*)}))'$$

where s^* means the meteorological station that measures the wind with the largest impact on wave-height change at s ($s = 1, \ldots, 6$) meteorological stations, and $WS_t^{(s^*)}$ means WS_t at the station.

The value of s^* is chosen by a statistical method based on measured data. It is defined as the value of s which minimizes the mean squared errors on forecasts made one-step ahead. Let $WS_t^{(s)}$ and $WD_t^{(s)}$ be wind speed and wind direction data, respectively, measured at the sth meteorological station. We first obtain forecasts of WH_t, one-step ahead in time, based on $\{WS_t^{(s)}\}$ and $\{WD_t^{(s)}\}$ ($s = 1, \ldots, 6$), say $\widetilde{WH}_{t+1}^{(s)}$ ($t = 1, \ldots, T-1$). The forecasts are obtained by fitting (8) to the sequence constructed by

$$\boldsymbol{y}_{t|s} = (\nabla WH_t,\ \nabla(\rho_t^{(s)} WS_t^{(s)} \cos(WD_t^{(s)})),\ \nabla(\rho_t^{(s)} WS_t^{(s)} \sin(WD_t^{(s)})),\ \cos(\mu_{(WD),t}^{(s)}),\ \sin(\mu_{(WD),t}^{(s)}))'.$$

Then, we choose the value of s^* by

$$s^* = \arg\min_{1 \le s \le 6} R(s, \tau(s))$$

where

$$R(s, \tau(s)) = \frac{1}{\tau(s)} \sum_{t=T-\tau(s)+1}^{T} (WH_t - \widetilde{WH}_t^{(s)})^2$$

where $\tau(s)$ means the local time interval, which depends on s. Thus, the forecasted value of WH_{T+l} ($l = 1, \ldots, L$) can be obtained by applying the predictor (9) to the sequence $\{\boldsymbol{y}_{t|s^*}; t = 1, \ldots, T\}$.

4. Evaluation of forecasting accuracies based on numerical experiments

An examination of the applicability of the spatiotemporal model, presented in the previous section, is required from the standpoint of forecasting accuracy. For this purpose, we carried out a forecasting experiment for the significant wave height by using several statistical models, and then compared forecasting accuracies among the models. The experimental procedure was as follows. First, the model was fit to the time series data of 100 samples (i.e., 100 hours) and forecasted values up to five steps ahead (i.e., 5 hours ahead) were determined. Next, the time point used for the starting forecast was changed randomly and the forecasting step above was repeated. After repeating the procedure, we obtained mean squared errors (MSE) and calculated the correlation between forecasted and actual values (COR), based on forecasted values and measured data. At the same time, the MSEs and CORs were also obtained using several traditional nonstationary time series models in a similar way. These values were compared between models to determine the class of models that gives the best forecasting accuracy. When we fit the models above, the order was determined by the Akaike Information Criterion (AIC).

4.1. Forecasting accuracy based on the surface wind monitored at a single meteorological station

We first investigate the case of forecasts based on the wind motions measured at Matsumae, the nearest location to the wave recorder. For this purpose, we obtained forecasted values of wave heights using wind speed and wind direction data measured at Matsumae. The statistical models introduced for comparisons are as follows.

(i) $WH_t = \sum_{i=1}^{p} \alpha_i WH_{t-i} + \varepsilon_{1,t}, \quad \varepsilon_{1,t} \sim WN(0, \sigma_1^2)$

(ii) $\nabla WH_t = \sum_{i=1}^{p} \beta_i \nabla WH_{t-i} + \varepsilon_{2,t}, \quad \varepsilon_{2,t} \sim WN(0, \sigma_2^2)$

(iii) $\boldsymbol{y}_t = A_1 \boldsymbol{y}_{t-1} + \cdots + A_p \boldsymbol{y}_{t-p} + \boldsymbol{\delta}_t, \qquad \boldsymbol{\delta}_t \sim WN(\boldsymbol{0}, \Sigma),$
$\boldsymbol{y}_t = (\nabla WH_t, \nabla WS_t)'$

(iv) $\boldsymbol{y}_t = A_1 \boldsymbol{y}_{t-1} + \cdots + A_p \boldsymbol{y}_{t-p} + \boldsymbol{\delta}_t, \qquad \boldsymbol{\delta}_t \sim WN(\boldsymbol{0}, \Sigma),$
$\boldsymbol{y}_t = (\nabla WH_t, \nabla(WS_t \cos(WD_t)))'$

(v) $\boldsymbol{y}_t = A_1 \boldsymbol{y}_{t-1} + \cdots + A_p \boldsymbol{y}_{t-p} + \boldsymbol{\delta}_t, \qquad \boldsymbol{\delta}_t \sim WN(\boldsymbol{0}, \Sigma),$
$\boldsymbol{y}_t = (\nabla WH_t, \nabla(\rho_t WS_t \sin(WD_t)), \sin(\mu_{(WD),t}))'$

(vi) $\boldsymbol{y}_t = A_1 \boldsymbol{y}_{t-1} + \cdots + A_p \boldsymbol{y}_{t-p} + \boldsymbol{\delta}_t, \qquad \boldsymbol{\delta}_t \sim WN(\boldsymbol{0}, \Sigma),$
$\boldsymbol{y}_t = (\nabla WH_t, \nabla(\rho_t WS_t \cos(WD_t)), \cos(\mu_{(WD),t}))'$

(i) and (ii) are models based on wave height only; the former is a stationary univariate AR(p) model and the latter is a nonstationary univariate ARIMA(p,1,0) model. (iii) is a nonstationary vector autoregressive model that takes into account changes in $\{WS_t\}$ and $\{WH_t\}$. Models (iv)-(vi) are nonstationary models that take into account both $\{WS_t\}$ and $\{WD_t\}$ as covariates. Note that (v) and (vi) belong to a class of model presented in the previous section.

	MSE					COR				
Model	**1-step**	**2-step**	**3-step**	**4-step**	**5-step**	**1-step**	**2-step**	**3-step**	**4-step**	**5-step**
(i)	0.039	0.089	0.141	0.195	0.224	0.982	0.955	0.927	0.886	0.862
(ii)	0.028	0.070	0.099	0.154	0.175	0.985	0.959	0.943	0.906	0.893
(iii)	0.030	0.072	0.101	0.153	0.166	0.984	0.960	0.944	0.912	0.903
(iv)	0.027	0.065	0.094	0.142	0.158	0.986	0.964	0.947	0.919	0.906
(v)	0.028	0.068	0.092	0.139	0.151	0.985	0.963	0.949	0.921	0.913
(vi)	0.027	0.064	0.092	0.140	0.157	0.986	0.965	0.950	0.919	0.908

Table 1. Forecasting accuracies of time series forecasts using each model

Table 1 shows the MSEs and CORs used with models (i)-(vi) for forecast up to five steps ahead, obtained by 130 repetitions. Comparison of (i) and (ii) shows that the forecast based on the nonstationary ARIMA(p,1,0) model is more accurate than a stationary AR model, which suggests that nonstationary models tends to give better forecasts than stationary models. Also, based on comparisons between (ii) and (iii) and between (ii) and (iv), we observe the tendency for (iii) and (iv) to give better forecasting accuracies than (ii), which also highlights the possibility of taking wind motion into account as a covariate contribution to improve forecasting accuracy. Comparisons between (iv) and (v) and between (iv) and (vi) suggest that a model which takes into account von Mises process on $\{WD_t\}$ will improve forecasting accuracies of (iii) and (iv), further. Based on the result above, it is determined that changes in the parameters of von Mises process assuming $\{WD_t\}$ tend to synchronize with $\{WS_t\}$ and $\{WH_t\}$.

4.2. Effect of spatiotemporal models on improvement of the forecasting accuracy

We next consider whether or not taking into account the wind motions measured at multiple meteorological stations contributes to the improvement of forecasting accuracies obtained in 4.1. To examine this point, we carried out forecasting experiments similar to those presented in 4.1. Additionally, we introduce the following spatiotemporal models for comparisons of forecasting accuracies.

vii) $\boldsymbol{y}_t = A_1\boldsymbol{y}_{t-1} + \cdots + A_p\boldsymbol{y}_{t-p} + \boldsymbol{\delta}_t, \quad \boldsymbol{\delta}_t \sim WN(\boldsymbol{0}, \Sigma),$
$\boldsymbol{y}_t = (\nabla WH_t, \nabla(WS_t^{(1)}\cos(WD_t^{(1)})), \ldots, \nabla(WS_t^{(6)}\cos(WD_t^{(6)})))'$

viii) $\boldsymbol{y}_t = A_1\boldsymbol{y}_{t-1} + \cdots + A_p\boldsymbol{y}_{t-p} + \boldsymbol{\delta}_t, \quad \boldsymbol{\delta}_t \sim WN(\boldsymbol{0}, \Sigma),$
$\boldsymbol{y}_t = (\nabla WH_t, \nabla(WS_t^{(s^*)}\cos(WD_t^{(s^*)})))'$

ix) $\boldsymbol{y}_t = A_1\boldsymbol{y}_{t-1} + \cdots + A_p\boldsymbol{y}_{t-p} + \boldsymbol{\delta}_t, \quad \boldsymbol{\delta}_t \sim WN(\boldsymbol{0}, \Sigma),$
$\boldsymbol{y}_t = (\nabla WH_t, \nabla(\rho_t^{(s^*)}WS_t^{(s^*)}\sin(WD_t^{(s^*)})), \sin(\mu_{(WD),t}^{(s^*)}))'$

x) $\boldsymbol{y}_t = A_1\boldsymbol{y}_{t-1} + \cdots + A_p\boldsymbol{y}_{t-p} + \boldsymbol{\delta}_t, \quad \boldsymbol{\delta}_t \sim WN(\boldsymbol{0}, \Sigma),$
$\boldsymbol{y}_t = (\nabla WH_t, \nabla(\rho_t^{(s^*)}WS_t^{(s^*)}\cos(WD_t^{(s^*)})), \cos(\mu_{(WD),t}^{(s^*)}))'$

Table 2 shows the MSEs and CORs obtained in the forecasting experiments above. (vii) is a standard vector autoregressive model based on multivariate wind speed and wind direction

	MSE					COR				
Model	**1-step**	**2-step**	**3-step**	**4-step**	**5-step**	**1-step**	**2-step**	**3-step**	**4-step**	**5-step**
(vii)	0.033	0.067	0.097	0.142	0.161	0.982	0.963	0.947	0.918	0.905
(viii)	0.027	0.067	0.094	0.136	0.153	0.986	0.965	0.952	0.927	0.917
(ix)	0.025	0.065	0.086	0.134	0.149	0.986	0.964	0.953	0.923	0.913
(x)	0.024	0.065	0.091	0.125	0.149	0.987	0.964	0.950	0.929	0.913

Table 2. Forecasting accuracies of spatiotemporal forecasts using each model

time series data measured at six meteorological stations. The results show that the forecasting accuracy of (vii) tends to become worse than forecasts based on a single meteorological station, as investigated in 4.1. This is likely because this class of model tends to have a large number of parameters that need to be estimated, which leads to negative impacts on forecasting accuracy. On the other hand, (viii) has fewer parameters than (vii), which leads to improved forecasting results as shown in Table 1. Furthermore, the class of the proposed models, (ix) and (x), contributes to the improvement of forecasting accuracies by (viii), which gives the best forecasting accuracy in our experiments.

5. Applying spatiotemporal modeling for wave-height forecasts

5.1. Robustness on wave-height forecasts over four seasons

In Japan, there are unique pressure pattern characteristics for each season, and it is therefore necessary to examine the applicability of the proposed model throughout the year. The purpose of this section is to investigate whether the model provides a robust forecast of wave height over the four seasons.

Figures 6-8 display, respectively, time series for the one-third significant wave height, wind speed and wind direction, in the spring (Apr. 1 - May 31), summer (Jul. 1-Aug. 31), autumn (Oct. 1 - Nov. 31) and winter (Jan. 1 - Feb.28), measured in Matsumae-oki and Matsumae. Overall, the characteristics of the changes are different for each season. Particularly in winter, the latent stochastic abilities differ from those in the other seasons, under a background of strong stable seasonal winds blowing from the northwest.

We carried out forecasting experiments similar to those presented in 4.1 and 4.2. In this experiment, some of the seven models introduced in 4.1 and 4.2 were adopted, and then their MSEs and CORs were compared for each season. More specifically, we adopted models (i)-(iv) from the time series models introduced in 4.1, and (vii), (viii) and (x) from the spatiotemporal models in 4.2.

Table 3 shows the MSEs obtained from forecasting experiments for each season. In spring, summer and autumn, the proposed spatiotemporal model (x) was evaluated as having an effective model structure for robust forecast, in the sense that it tends to give the best MSEs of the seven models tested. Note that, as for the winter forecast, there is no clear improvement on the MSEs. This tendency is presumed to result from the wind direction in this season, which is generally from the northwest with the degree of fluctuation that is smaller than in the other three seasons.

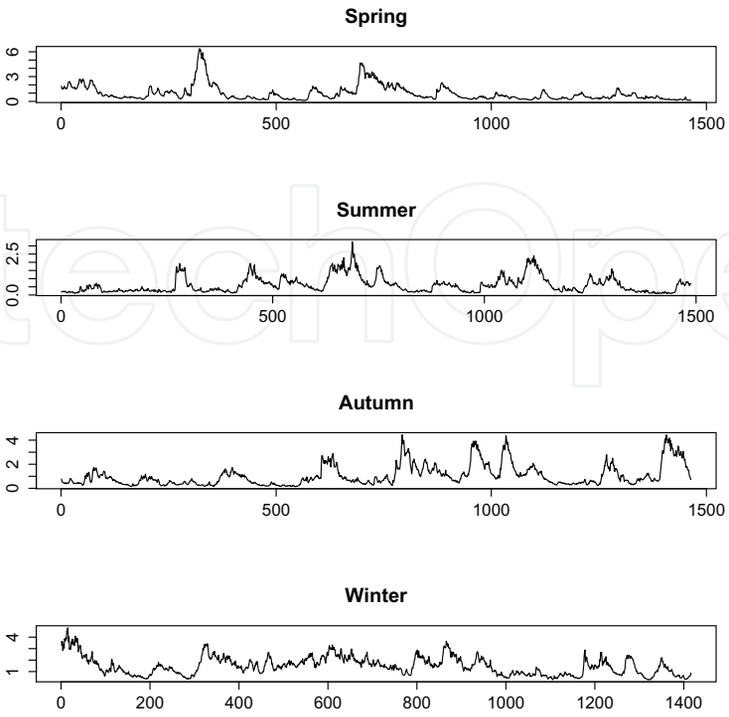

Figure 6. Changes in 1/3 significant wave height (m) for the four seasons (Matsumae-oki)

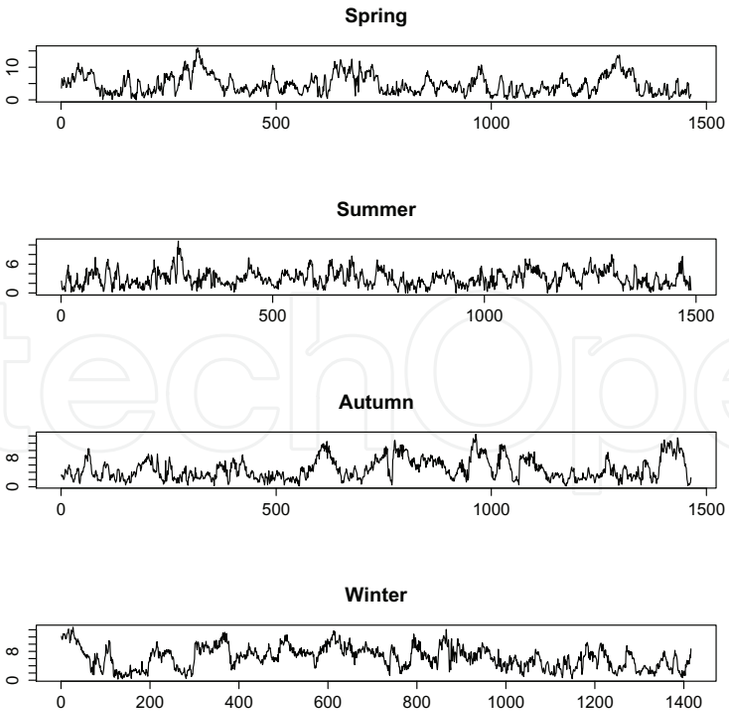

Figure 7. Changes in wind speed (m/s) for the four seasons (Matsumae)

A) Spring

Model	Region(s)	1-step	2-step	3-step	4-step	5-step
(i)	1	0.039	0.089	0.141	0.195	0.224
(ii)	1	0.028	0.070	0.099	0.154	0.175
(iii)	1	0.030	0.072	0.101	0.153	0.166
(iv)	1	0.027	0.065	0.094	0.142	0.158
(vii)	6	0.033	0.067	0.097	0.142	0.161
(viii)	6	0.027	0.067	0.094	0.136	0.153
(x)	6	0.024	0.065	0.091	0.125	0.150

B) Summer

Model	Region(s)	1-step	2-step	3-step	4-step	5-step
(i)	1	0.015	0.025	0.033	0.048	0.073
(ii)	1	0.011	0.015	0.023	0.040	0.059
(iii)	1	0.011	0.014	0.023	0.039	0.058
(iv)	1	0.011	0.014	0.022	0.038	0.056
(vii)	6	0.012	0.017	0.025	0.040	0.056
(viii)	6	0.012	0.014	0.022	0.036	0.054
(x)	6	0.012	0.016	0.022	0.036	0.053

C) Autumn

Model	Region(s)	1-step	2-step	3-step	4-step	5-step
(i)	1	0.024	0.091	0.139	0.222	0.267
(ii)	1	0.014	0.052	0.087	0.145	0.180
(iii)	1	0.013	0.050	0.083	0.139	0.171
(iv)	1	0.014	0.051	0.084	0.142	0.173
(vii)	6	0.018	0.056	0.088	0.132	0.157
(viii)	6	0.014	0.051	0.084	0.134	0.158
(x)	6	0.013	0.045	0.081	0.129	0.162

D) Winter

Model	Region(s)	1-step	2-step	3-step	4-step	5-step
(i)	1	0.021	0.051	0.088	0.119	0.159
(ii)	1	0.021	0.049	0.086	0.114	0.154
(iii)	1	0.021	0.047	0.081	0.108	0.146
(iv)	1	0.020	0.047	0.081	0.109	0.147
(vii)	6	0.023	0.050	0.090	0.122	0.157
(viii)	6	0.022	0.049	0.085	0.113	0.148
(x)	6	0.021	0.047	0.084	0.110	0.147

Table 3. Comparisons of MSEs for all seasons

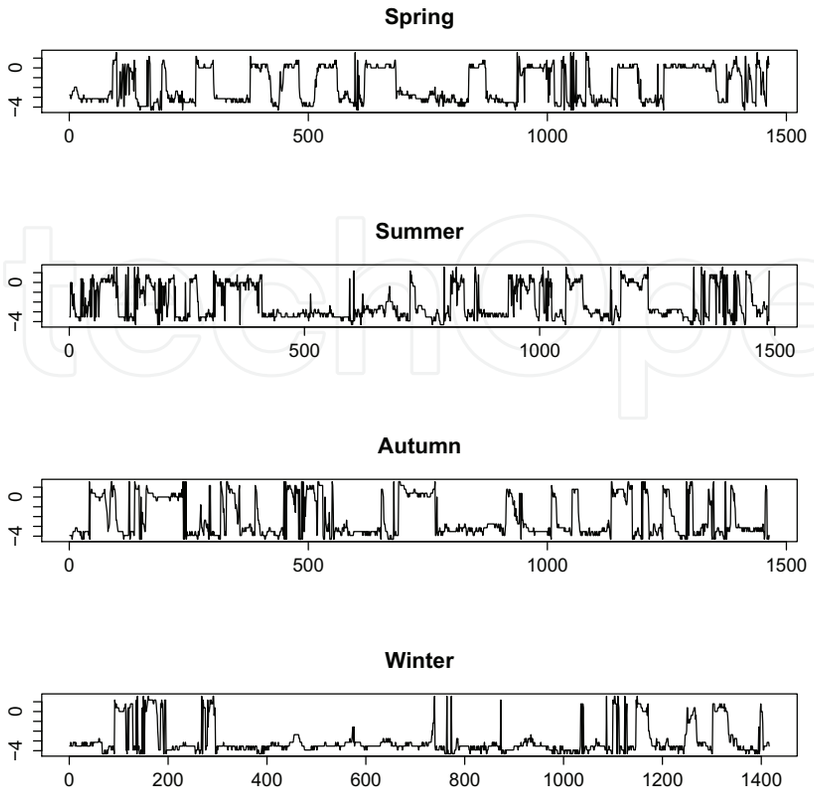

Figure 8. Changes in wind direction (rad.) for the four seasons (Matsumae)

5.2. Application of the model to estimate the impacts of wind flow on wave height

One of on the reasons why wave development phenomena are of interest is to improve understanding of how the direction of wind flow can impacts wave heights. To examine the applicability of the spatiotemporal model developed here, we estimate the wind flow above by applying the model. Figure 9 displays histograms showing wind direction for the four seasons, as observed in the data measured at six meteorological stations. Note that the horizontal axis corresponds to the wind direction shown at 16 azimuths, where 1, 5, 9, 13 corresponds to north, east, south and west, respectively. And Figure 10 shows histograms of the estimated values of s^* obtained using the proposed model (x). Here "MA", "OK", "ES", "MO", "HA" and "OH" correspond to the meteorological stations located at Matsumae, Okushiri, Esashi, Mori, Hakodate and Ohma, respectively.

We have examined whether or not it is possible to estimate wind flow that results in a large impact on wave height using the histograms shown in Figure 10. In spring, Figure 10 suggests that the meteorological stations at Hakodate, Matsumae and Esashi are capable of measuring the wind flow that significantly impacts wave motion at Matsumae-oki. In addition, Figure 9 shows that wind flows from the east and west are highly probable. For the case of westerly winds, based on Figure 1, wind motions measured over Okushiri, Esashi and Matsumae are thought to be highly correlated with wave-height changes at Matsumae-oki, where the open

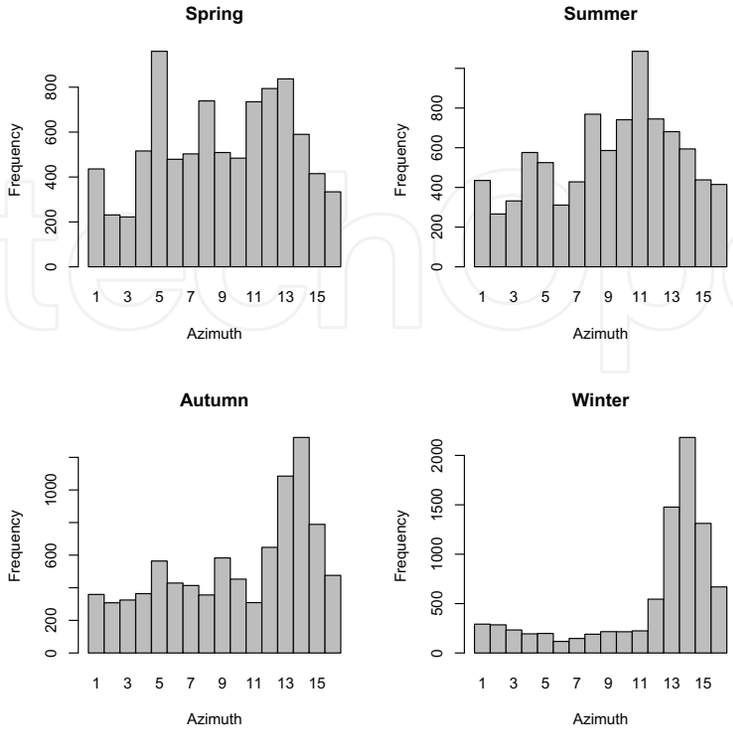

Figure 9. Histograms of wind directions for the four seasons

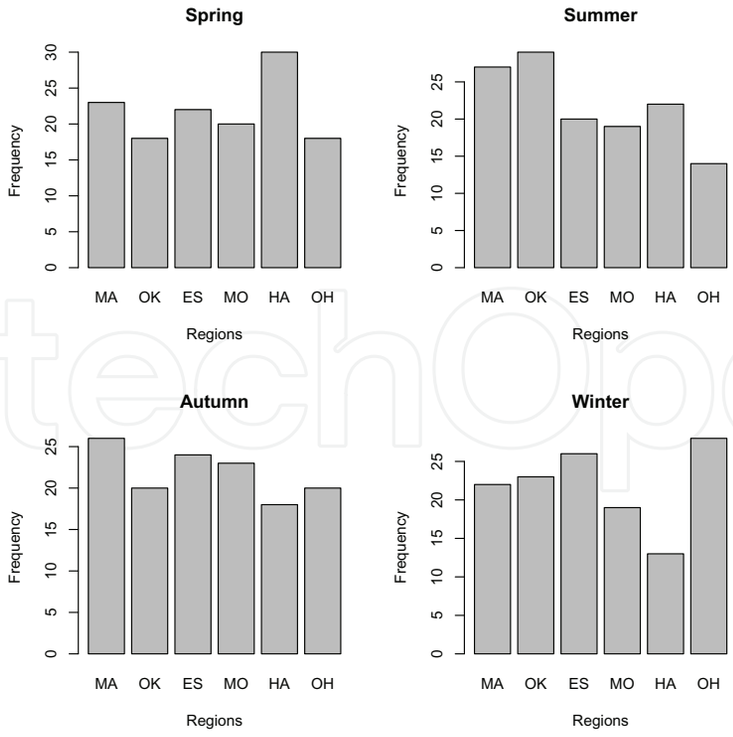

Figure 10. Histograms of estimated values for s^* for the four seasons

sea lies directly to the west of the towns above. In contrast, when the wind blows from the east, the wind motion over Hakodate, Ohma and Matsumae is thought to correlate with the wave height where the open sea lies directly to the east of these towns. Therefore, the evaluation of the data shows that the estimated stations in Figure 10, Hakodate, Matsumae and Esashi, can be classified with the five stations above. In summer, the dominant winds are southwesterlies (Figure 9). In such winds, the wind motions over Okushiri, Esashi, Matsumae and Hakodate are expected to correlate with the wave motion over Matsumae-oki, because there is open sea with sufficient fetch to the southwest of that location. In contrast, Figure 10 suggests that Matsumae, Okushiri and Hakodate are estimated as s^*, which is consistent with the towns above. In winter, strong seasonal winds are mainly northwesterlies. In this case, Ohma, Matsumae, Okushiri and Esashi are expected to have the best correlations with the wave motion for similar reasons as before. Figure 10 shows that Ohma, Esashi and Okushiri are estimated as s^*, and can be classified with the towns above.

Based on the considerations presented above, meteorological station measurements of wind flow, presented in the histogram of s^*, are shown to be effective for estimating wave-height changes at Matsumae-oki.

6. Conclusion

In this chapter, we have developed a statistical spatiotemporal model for forecasting wave-height changes and then applied it to the wave-height forecasting problem based on spatiotemporal wind motions measured at multiple AMeDAS meteorological stations. The results of the forecasting experiments have shown that the spatiotemporal model, that takes wind speed and wind direction into account, can improve forecasting accuracy when general time series models are used.

The spatiotemporal model presented in this chapter assumes that changes in wind direction follow the von Mises process. It may be possible, however, to further improve the forecasting accuracy by considering a stochastic process that enables a more flexible expression of changes in direction. The model improvements, including the consideration of directional processes, are expected to contribute to a deeper understanding of the transitional phenomenon that link wind motion and wave development, as well as the spatiotemporal processes involved with wind motion.

Author details

Tsukasa Hokimoto

Graduate School of Mathematical Sciences, The University of Tokyo, Japan

References

[1] Athanassoulis, G.A., Stefanakos, C.N. (1995). A nonstationary stochastic model for long-term time series of significant wave height, *Journal of Geophysical Research*, 100(C8), 16149-16162.

[2] Box, G.E.P., Jenkins, G.M. (1976). *Time Series Analysis, Forecasting and Control* (revised edition), Holden-Day, San Francisco.

[3] Breckling, J. (1989). *The Analysis of Directional Time Series: Applications to Wind Speed and Direction*, Lecture Notes in Statistics, 61, Springer-Verlag, Berlin.

[4] Brockwell, P.J., Davis, R.A. (1996). *Introduction to Time Series and Forecasting*, Springer-Verlag, New York.

[5] Erdem, E., Shi, J. (2011). ARMA based approaches for forecasting the tuple of wind speed and direction, *Applied Energy*, vol. 88, issue 4, 1405-1414.

[6] Guedes Soares, C., Ferreira, A.M. (1996). Representation of non-stationary time series of significant wave height with autoregressive models, *Probabilistic Engineering Mechanics*, 11, 139-148.

[7] Hokimoto, T., Shimizu, K. (2008). An angular-linear time series model for waveheight prediction, *Annals of the Institute of Statistical Mathematics*, 60, 781-800.

[8] Hokimoto, T. (2012). *Prediction of wave height based on the monitoring of surface wind*, Ocenanography, Chapter 8, 169-188, InTech, Rijeka, Croatia.

[9] Johnson, R.A., Wehrly, T.E. (1978). *Some angular-linear distributions and related regression models*, Journal of the American Statistical Association, 73, 602-606.

[10] Liu, H., Erdem, E., Shi, J. (2011). Comprehensive evaluation of ARMA-GARCH(-M) approaches for modeling the mean and volatility of wind speed, *Applied Energy*, 88, 724-732

[11] Philippopoulos, K., Deligiorgi, D. (2009). Statistical simulation of wind speed in Athens, Greece based on Weibull and ARMA models, *International Journal of energy and environment*, Issue 4, Volume 3, 151-158

[12] Pierson, W.J., Neumann, G, and James, R.W. (1960). *Practical Methods for Observing and Forecasting Ocean Waves by Means of Wave Spectra and Statistics*, U.S. Navy Hydrographic Office; Reprint edition.

[13] Scotto, M.G., Guedes Soares, C. (2000). Modelling the long-term time series of significant wave height with non-linear threshold models, *Coastal Engineering*, 40, 313-327.

[14] Scheffner, N.W., Borgman, L.E. (1992). Stochastic time-series representation of wave data, *Journal of Waterway, Port, Coastal and Ocean Engineering*, 118 (4), 337-351.

[15] Spanos, P.D. (1983). ARMA algorithms for ocean wave modelling, *Journal of Energy Resources Technology*, 105, 300-309.

[16] Sverdrup, H.U., and Munk, W.H. (1947). *Wind Sea and Swell: Theory of Relation for Forecasting*, U.S. Navy Hydrographic Office, Washington, D.C., No. 601.

[17] Tol, R.S.J. (1997). Autoregressive conditional heteroscedasticity in daily wind speed measurements, *Theoretical and Applied Climatology*, 56, 113-122.

IntechOpen